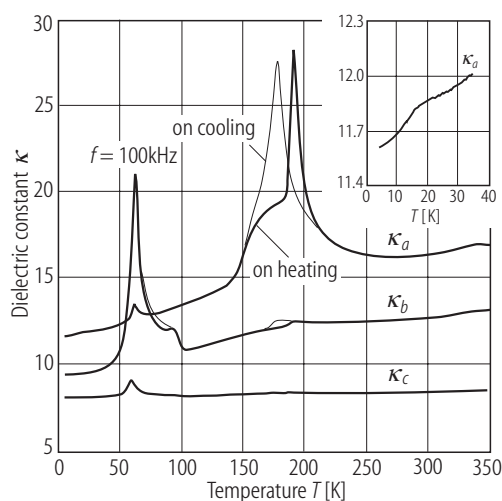
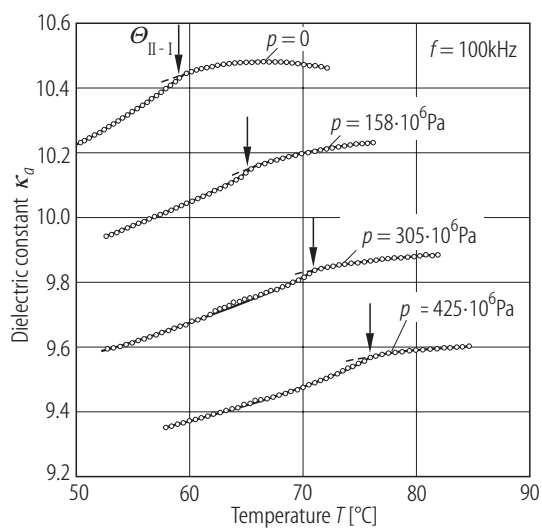


**Fig. 39A-14-001.** Rb<sub>2</sub>CoBr<sub>4</sub>.  $\Theta$  vs.  $p$  [90Ges2]. Vertical bars show thermal hysteresis of the transition. III–II phase transition was observed up to about 150 MPa. Existence of pressure-induced phase was suggested at higher pressures.



**Fig. 39A-14-002.** Rb<sub>2</sub>CoBr<sub>4</sub>.  $\kappa_a$ ,  $\kappa_b$ ,  $\kappa_c$  vs.  $T$  [91Yam].  $f = 100$  kHz. Insert:  $\kappa_a$  vs.  $T$  below 35 K.



**Fig. 39A-14-003.**  $\text{Rb}_2\text{CoBr}_4$ .  $\kappa_d$  vs.  $T$  [90Ges2]. Parameter:  $p, f = 100 \text{ kHz}$ .

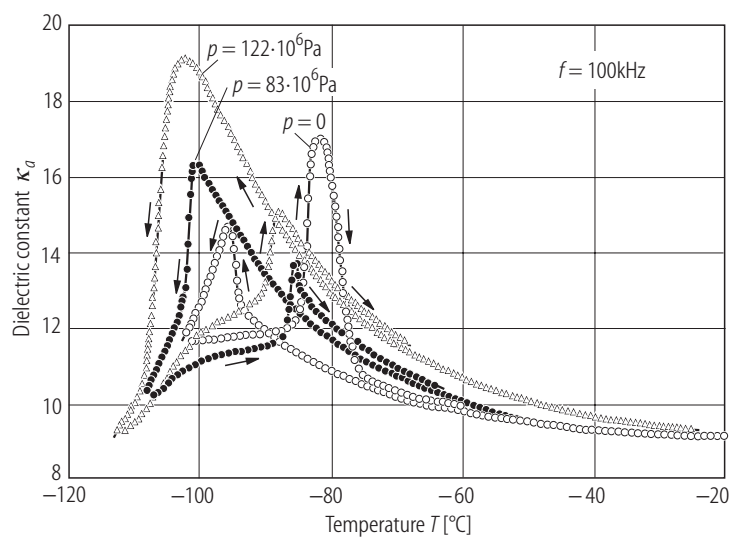


**Fig. 39A-14-004.**  $\text{Rb}_2\text{CoBr}_4$ .  $\kappa_d$  vs.  $T$  [90Ges2]. Parameter:  $p, f = 100 \text{ kHz}$ .

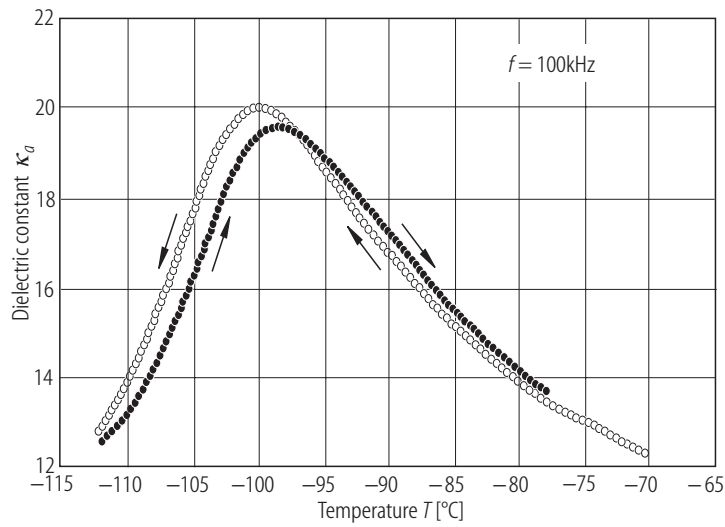


**Fig. 39A-14-005.**  $\text{Rb}_2\text{CoBr}_4$ .  $\kappa_a$  vs.  $T$  at  $p = 159$  MPa [90Ges2].  $f = 100$  kHz.

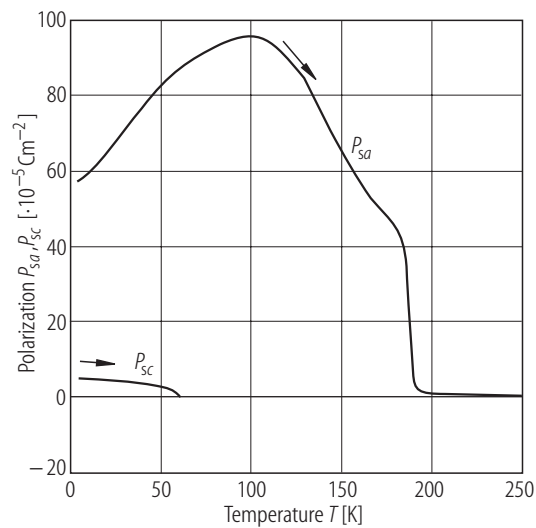


**Fig. 39A-14-006.**  $\text{Rb}_2\text{CoBr}_4$ .  $P_{sa}$ ,  $P_{sc}$  vs.  $T$  [91Yam].  $P_{sa}$ ,  $P_{sc}$ : spontaneous polarization along the  $a$  and  $c$  axes, respectively. Pyroelectric charge measurements on heating.

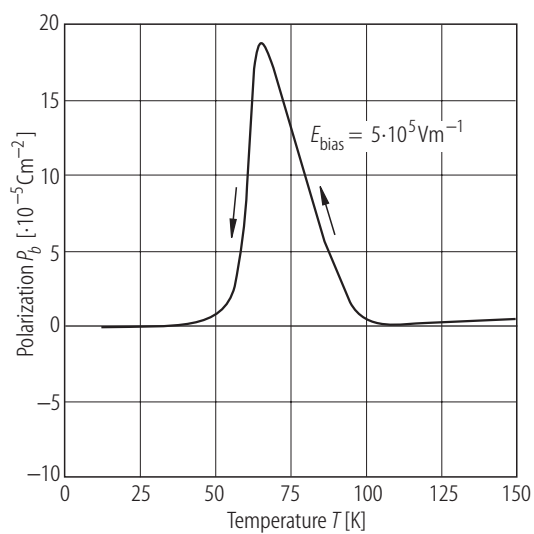


**Fig. 39A-14-007.** Rb<sub>2</sub>CoBr<sub>4</sub>.  $P_b$  vs.  $T$  [91Yam].  $P_b$ : polarization induced by electric field along the  $b$  axis,  $E_{\text{bias}} = 5 \cdot 10^5 \text{ V m}^{-1}$ . Pyroelectric charge measurements on cooling.

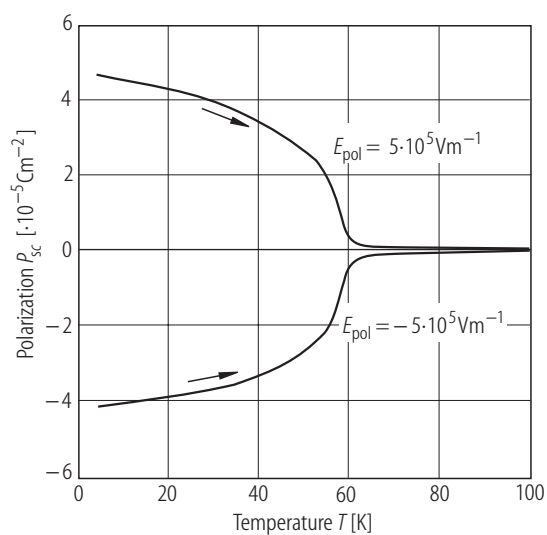


**Fig. 39A-14-008.** Rb<sub>2</sub>CoBr<sub>4</sub>.  $P_{\text{sc}}$  vs.  $T$  [91Yam].  $P_{\text{sc}}$ : spontaneous polarization along the  $c$  axis,  $E_{\text{pol}}$ : poling field. Pyroelectric charge measurements on heating.

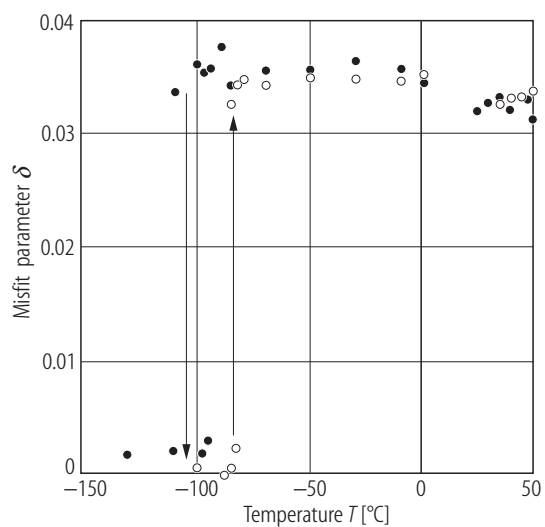


**Fig. 39A-14-009.**  $\text{Rb}_2\text{CoBr}_4$ .  $\delta$  vs.  $T$  [87Kas]. X-ray diffraction.  $\delta$  is defined by  $k_z = (1/3 - \delta)c_0^*$ , and  $c_0^*$  represents the reciprocal lattice constant in phase I.